Earthquakes and Structures, *Vol. 21, No. 5 (2021) 531-549*
https://doi.org/10.12989/eas.2021.21.5.531

Seismic analysis and performance for stone pagoda structure under Gyeongju earthquake in Korea

Ho-Soo Kim[a], Dong-Kwan Kim[b] and Geon-Woo Jeon[*]

Department of Architectural Engineering, Cheongju University, 298, Daeseong-ro, Cheongwon-gu, Cheongju-si, Chungcheongbuk-do, Republic of Korea

(Received August 18, 2021, Revised September 29, 2021, Accepted November 18, 2021)

Abstract. Analytical models were developed and seismic behaviors were analyzed for a three-story stone pagoda at the Cheollyongsa temple site, which was damaged by the Gyeongju earthquake of 2016. Both finite and discrete element modeling were used and the analysis results were compared to the actual earthquake damage. Vulnerable parts of stone pagoda structure were identified and their seismic behaviors via sliding, rocking, and risk analyses were verified. In finite and discrete element analyses, the 3F main body stone was displaced uniaxially by 60 and 80 mm, respectively, similar to the actual displacement of 90 mm resulting from the earthquake. Considering various input conditions such as uniaxial excitation and soil-structure interaction, as well as seismic components and the distance from the epicenter, both models yielded reasonable and applicable results. The Gyeongju earthquake exhibited extreme short-period characteristics; thus, short-period structures such as stone pagodas were seriously damaged. In addition, we found that sliding occurred in the upper parts because the vertical load was low, but rocking predominated in the lower parts because most structural members were slender. The third-floor main body and roof stones were particularly vulnerable because some damage occurred when the sliding and rocking limits were exceeded. Risk analysis revealed that the probability of collapse was minimal at 0.1 g, but exceeded 80% at above 0.3 g. The collapse risks at an earthquake peak ground acceleration of 0.154 g at the immediate occupancy, life safety, and collapse prevention levels were 90%, 52%, and 6% respectively. When the actual damage was compared with the risk analysis, the stone pagoda retained earthquake-resistant performance at the life safety level.

Keywords: analytical model; discrete element analysis; finite element analysis; Gyeongju earthquake; seismic performance; stone pagoda

1. Introduction

In Korea, the frequency of strong earthquakes (magnitude ≥ 5.0) is increasing; examples include the Gyeongju earthquake of 2016 ($M_w = 5.8$) and the Pohang earthquake of 2017 ($M_w = 5.4$). These earthquakes damaged over 100 buildings, some of which had cultural significance. Because stone pagodas are masonry stacks, they are vulnerable to lateral loads that cause the stone components to slide, rotate, separate, or break. To evaluate such damage, structural modeling and analysis are required. Pena *et al.* (2010) subjected the Qutb Minarto to nonlinear static and dynamic analyses using seismic waves matching the design spectrum of the Indian standard. Nonlinear dynamic analysis reliably evaluated the seismic performance of a masonry tower. Yurdakul *et al.* (2021) used SAP 2000 software to structurally model a historical minaret using a finite element method that included both solid and shell elements. Dynamic behaviors during the Erzincan, Kocaeli-Duzce, and Van-Ercis earthquakes were analyzed. Hejazi *et al.* (2015) performed nonlinear finite element analysis based on the seismic design standard of Iran and analyzed tower behavior and damage based on seismic intensity. Preciado *et al.* (2017) performed linear and nonlinear finite element analyses (with or without vertical, external prestressing reinforcement) of the Torre Grossa medieval tower and analyzed its behavior. Micelli *et al.* (2020) performed nonlinear finite element analysis of the Raimondellos tower and analyzed the dynamic behavior and failure mechanisms. Adam *et al.* (2020) performed nonlinear analysis of a historical masonry minaret using the Turkish earthquake code, and Taha Yasin Altiok and Ali Demir (2021) estimated the collapse mechanism of a historical masonry minaret. Thus, most studies that performed structural modeling have used finite element analysis to analyze the behavioral characteristics of masonry structures built of bricks and blocks. However, such structures exhibit discontinuous surface contacts, and it is not easy to model contact surface discontinuities using a general finite element analysis. In particular, the construction of Korean stone pagodas differs from that of masonry structures elsewhere, necessitating a dedicated method of modeling and structural analysis. In addition, it is difficult to evaluate seismic performance because Korea lacks earthquake-specific structural safety standards for

*Corresponding author, Ph.D.
E-mail: rjsdn1591@naver.com
[a]Ph.D. Professor
E-mail: hskim@cju.ac.kr
[b]Ph.D. Assistant Professor
E-mail: dkkim17@cju.ac.kr

ISSN: 2092-7614 (Print), 2092-7622 (Online)

Table 1 The epicenter depths of Korean earthquakes of magnitude greater than 5.0

No	Magnitude	Date	Location	Depth (km)
1	5.2	2004/05/29	74 km southeast of Uljin-gun, Gyeongsangbuk-do	3.7
2	5.1	2014/04/01	100 km northwest of Seogyeokryeolbi-do, Taean-gun, Chungcheongnam-do	12.6
3	5.0	2016/07/05	52 km east of Dong-gu, Ulsan	10.0
4	5.0	2003/03/30	88 km southwest of Baengnyeong Island, Incheon	4.5
5	5.0	1978/10/07	3 km east of Hongseong-gun, Chungcheongnam-do	10.0

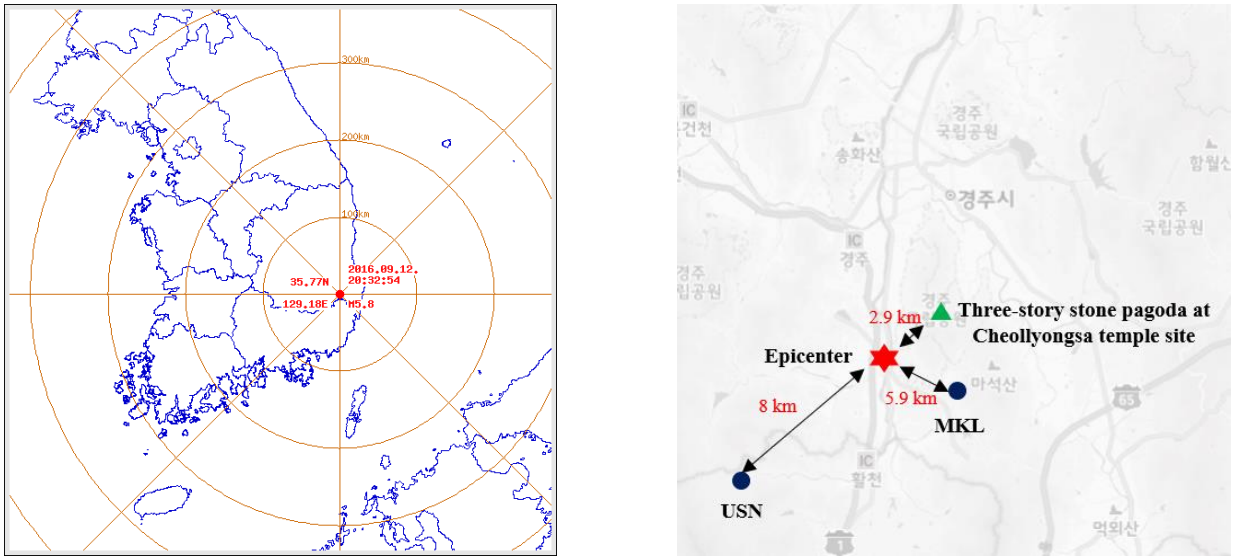

(a) Epicenter of the Gyeongju earthquake (magnitude 5.8) (b) Earthquake stations around the epicenter

Fig. 1 The Gyeongju earthquake

Table 2 Earthquake stations in Gyeongju

No.	Code	Latitude (°N)	Longitude (°E)	Altitude (m)
1	MKL	35.7322	129.2419	187
2	HDB	35.7337	129.3991	146
3	DAG2	35.7685	128.8970	283
4	PHA2	36.1929	129.3708	46
5	GKP1	35.8893	128.6061	56

masonry stone pagodas. Thus, the criteria applicable to an unreinforced masonry shear wall system was used.

Here, this study selected a three-story stone pagoda at the Cheollyongsa temple site, which was dismantled because of major damage caused by the Gyeongju earthquake. Appropriate analytical models were established and structural analyses using this and standard techniques were performed. Both finite and discrete element models were employed and then the results to the actual earthquake damage were compared. Sliding, rocking, and risk analyses were applied to identify the vulnerable parts at risk during earthquakes, and their seismic performances were analyzed.

2. Damage caused by the Gyeongju earthquake

2.1 Characteristics of the Gyeongju earthquake

The Gyeongju earthquake of September 12, 2016 occurred 15 km underground, and was thus deeper than the average depth of 8.16 km of an earthquake of magnitude 5.0 or more in Korea. At an observatory near the epicenter, the earthquake duration was approximately 5~7 s, thus shorter than the 20~170 s of large-scale earthquakes in Japan (Ministry of Public Safety and Security 2017). In addition, based on the short earthquake duration, the shock wave energy was concentrated, causing great damage to the short-period structure. Table 1 shows the epicenter depths of Korean earthquakes of magnitude greater than 5.0 (Ministry of Public Safety and Security 2017).

We obtained earthquake acceleration data from nearby Gyeongju observatories operated by the Korea Meteorological Administration and the Korea Institute of Geoscience and Mineral Resources. The acceleration data were converted into velocity data and then applied to numerical analysis. Fig. 1 and Table 2 detail seismic stations near Gyeongju.

Analysis of seismic waves observed at 5.9~22 km from the epicenter (measured from the ground down) revealed that the peak ground acceleration was 0.404 g. This is the largest earthquake recorded to date in Korea; the data are therefore very important to Korean seismic engineers. The

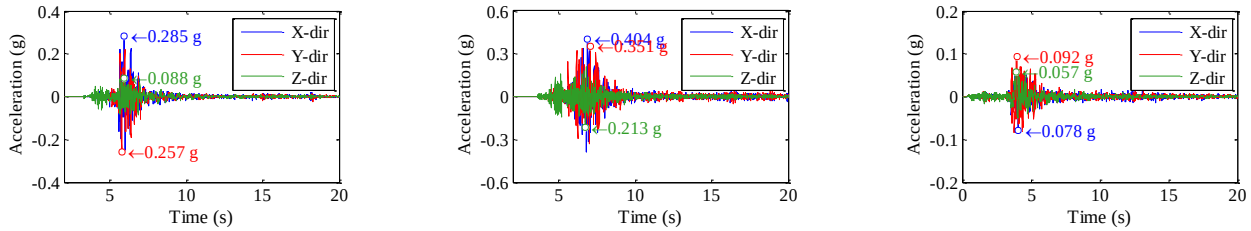

(a) MKL record (b) USN record (c) DKJ record

Fig. 2 Gyeongju earthquake records

Table 3 Stone pagodas damaged by the Gyeongju earthquake

Name	Damage
Stone brick pagoda of Bunhwangsa temple	• Some cracks and exterior wall flaking • Inclination (2 cm)
Cheomseongdae observatory	Separation of the southeast contact of an upper member (5cm) (Fig. 3(b)) South upper member deformed to the north direction (3.8 cm)
Five-story stone pagoda in Nawon-ri	• Joint crack in the 1F main body stone
East and west three-story stone pagodas in Cheongun-dong	• Breakage of upper regions
Three-story stone pagoda of Pyochungsa temple	• Breakage of roofing tiles
East and west three-story stone pagodas of Unmunsa temple	• East pagoda: Collapse of upper member West pagoda: Tilting
Three-story stone pagoda in Yongmyeong-ri	• Protrusion of the upper region
Three-story stone pagoda at Cheollyongsa temple site	• Westward deformation 9 cm to the west of the third floor (3F) main body and roof stones (Fig. 3(a)) Separation of 2F roof stones
East and west three-story stone pagodas at Wonwonsa temple site	• Breakage of the roof stone edge of the east-facing pagoda
Three-story stone pagoda at Changnimsa temple site	• Breakage of roof stone
Three-story stone pagoda at the third temple site in Namsan mountain	• Counterclockwise rotation and westward deformation of the decorative top Sliding of the 3F main body stone
East and west three-story stone pagodas of Yeombulsa temple	• Separation of the 3F main body stone
Three-story stone pagoda at the second temple site in Bipagok valley of Namsan mountain	• Breakage of the lime bonding agent Counterclockwise rotation of the main body and roof stones of the first to the third story (Fig. 3(c))
Three-story stone pagoda at the third temple site in Jiamgok valley on Namsan mountain	• Southward sliding 2 cm of the 3F main body and roof stones Southward sliding 5 cm and counterclockwise rotation of the decorative top (Fig. 3(d))

peak ground acceleration measured at the Myunggye-ri observatory (MKL) 5.9 km from the epicenter was 0.257~0.285 g horizontally and 0.088 g vertically, while the peak ground acceleration at the Ulsan observatory (USN) 8.0 km from the epicenter was 0.351~0.404 g horizontally and 0.213 g vertically. Although the Ulsan observatory was located further from the epicenter, vibration was amplified by the ground characteristics near the observatory. The peak ground acceleration at the Dukjeong-ri observatory (DKJ) 22 km from the epicenter was 0.078~0.092 g horizontally and 0.057 g vertically. Seismic activity generally decreased as the waves moved away from the epicenter (Ki-Hyun Jeong and Han-Seon Lee 2018).

2.2 Damage to stone pagoda structures

In Gyeongju and surrounding areas, 54 state-designated cultural properties and 50 provincially designated cultural properties (i.e., 104 total properties) were damaged. Most pagoda damage occurred in the upper parts. The upward decrease in the size of components and contact surfaces results in rotation and movement of the roof and upper main body stones, as well as dislocation of the decorative top. The stone pagoda structures on Mt Namsan were located approximately 2.9 km from the epicenter and experienced relatively heavy damage. The stone pagodas damaged by the earthquake are listed in Table 3.

3. Seismic analysis and verification

3.1 Target structures

Various techniques including finite and discrete element analysis can be used to model stone pagodas subject to earthquake damage. In partiucular, it is necessary to establish reliable structural models because the results of such analysis depend greatly on the input variables. We built a model of the three-story stone pagoda at Cheollyongsa temple site, where the 3F roof and 3F main body stones slipped by approximately 9 cm. Table 4 shows construction details and Fig. 4 shows elevations of the stone pagoda (National Research Institute of Cultural Heritage 2009).

(a) Three-story stone pagoda at Cheollyongsa temple site

(b) Cheomseongdae observatory

(c) Three-story stone pagoda at the second temple site in Bipagok valley on Mt Namsan

(d) Three-story stone pagoda at the third temple site in Jiamgok valley on Mt Namsan

Fig. 3 Stone pagoda damage caused by the Gyeongju earthquake

Table 4 Summary of the three-story stone pagoda construction at Cheollyongsa temple site

Classification			Member name	Quantity (sheets)
Member	Foundation		Gapseok	4
			Myeonseok	8
			Foundation stone	5
	Body	Third story	Roof stone	1
			Body stone	1
		Second story	Roof stone	1
			Body stone	1
		First story	Roof stone	1
			Body stone	1
	Upper part		Decorative top	16
Total				39

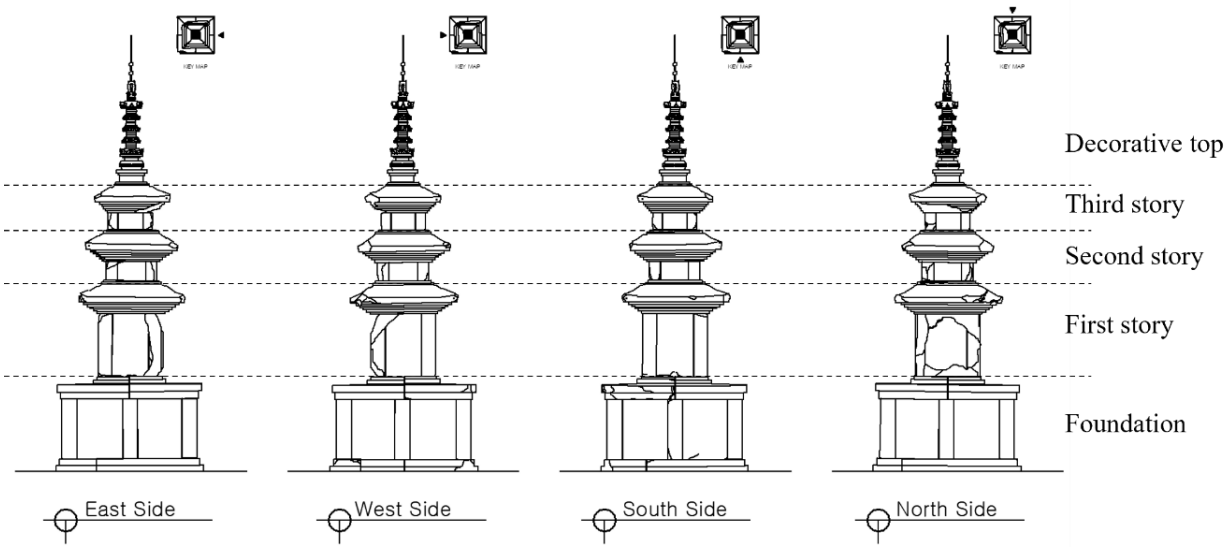

Fig. 4 Elevations of the three-story stone pagoda

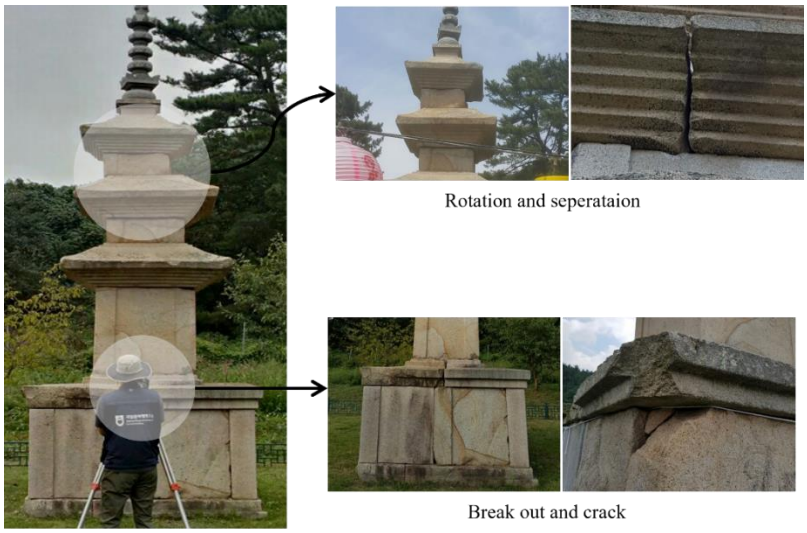

Fig. 5 Earthquake damage to the three-story stone pagoda of Cheollyongsa temple site

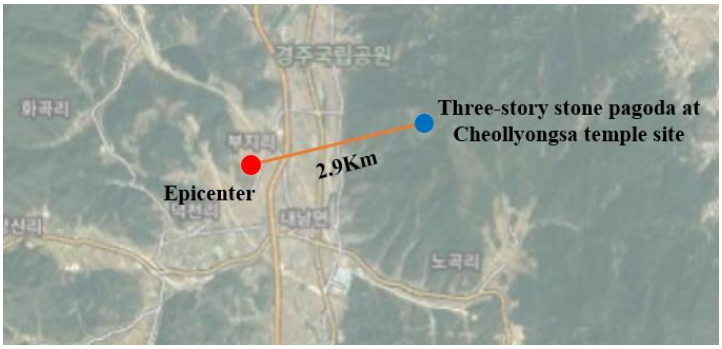

Fig. 6 Distance between the Cheollyongsa temple site and the epicenter

Fig. 7 The epicenter and nearby observatories

The stone pagoda structure is of slender construction; the 1F main body stone is much more slender than the 2F and 3F main body stones. The 3F main body and roof stones moved approximately 9 cm westward, while the decorative top rotated clockwise. The size of members and contact surfaces decrease rapidly upward; thus, the upper part was greatly deformed. Furthermore, because the stone pagoda structure was located near the epicenter, the earthquake caused significant damage, as shown in Fig. 5. Fig. 6 shows the distance between the Cheollyongsa temple site and the epicenter.

3.2 Input seismic waves

The input seismic records feature large x-direction components of both horizontal elements recorded at the

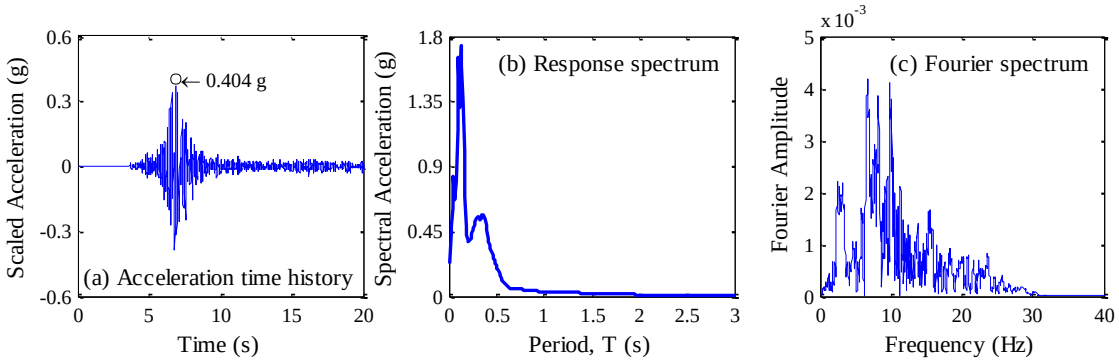

Fig. 8 Input acceleration

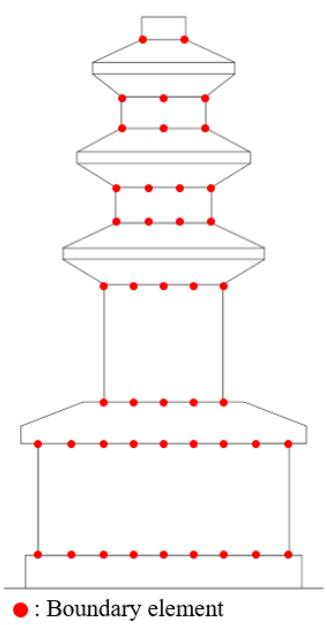

(a) Boundary elements

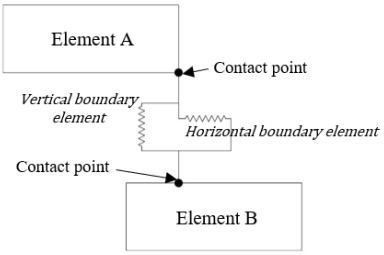

(b) Vertical and horizontal boundary elements

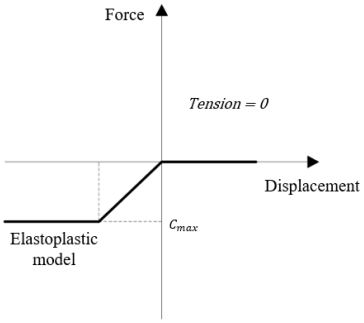

(c) Nonlinear characteristics of vertical boundary elements

Fig. 9 Modeling of discontinuous surface boundaries

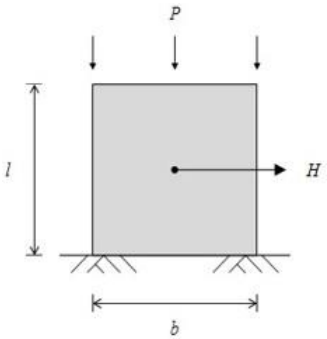

(a) Single stone member

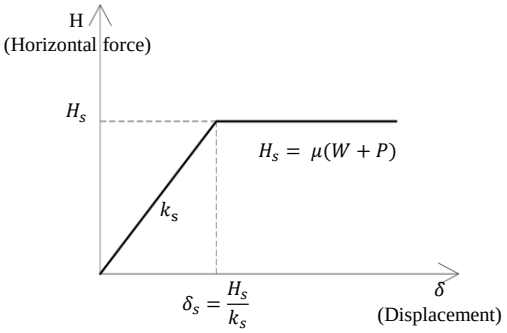

(b) Horizontal stiffness model that considers sliding

Fig. 10 Horizontal stiffness related to sliding

USN station 8.0 km from the epicenter; the distances of various stations from the epicenter are shown in Fig. 7. Although the MKL observatory was located only 5.9 km from the epicenter, the USN station record reflects the effect of the S_4 ground type, which was considered suitable for the construction of a three-story stone pagoda at the Cheollyongsa temple site (Ministry of Public Safety and Security 2017). Because the stone pagoda was located 2.9 km from the epicenter, we reflected the effect of distance on earthquake reduction. To this end, we gradually increased the USN seismic record and applied incremental non-linear dynamic analysis to observe the resulting structural damage.

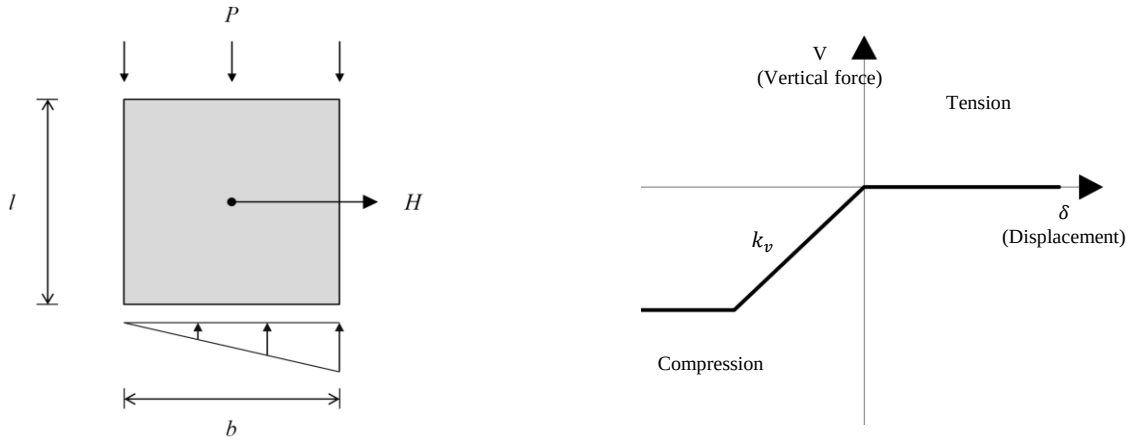

(a) Lower-level stress distribution when uplift develops (b) Vertical stiffness model that considers uplift

Fig. 11 Vertical stiffness related to uplift

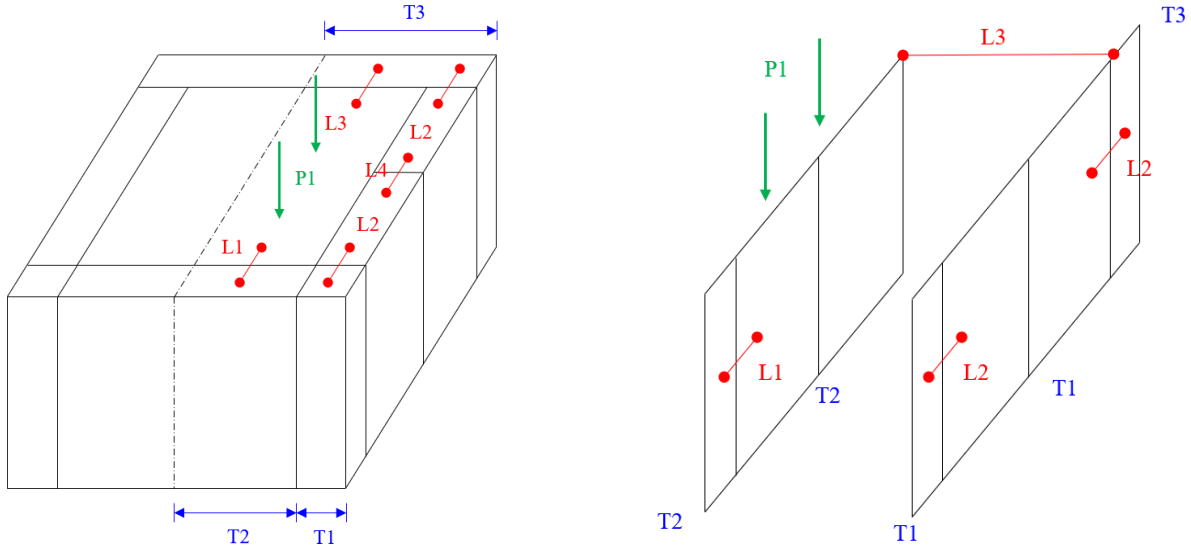

(a) Typical 3D model (b) 2D finite element model

Fig. 12 A 2D finite element model featuring multiple members

3.3 Finite element analysis

3.3.1 Analytical model

We used the OPENSEES program to perform nonlinear structural analysis of the stone pagoda and obtained its nonlinear properties based on a comparison with actual damage (OpenSees 2020). In addition, we carefully analyzed the behavior of the structure at the discontinuous surface between stones undergoing rigid body motion to reflect this aspect in the analytical model. Boundary modeling of discontinuities requires that transmission of only the compressive force between two stones is permitted and tensile force transmission is prohibited. Here, each boundary surface can be modeled by a zero-length element and applied to a vertical boundary element.

The behavioral characteristics of a single stone member can be confined to sliding and rocking, and the nonlinear boundary conditions imposed on the contact surfaces are consistent with these states. As shown in Fig. 10(a), the horizontal force (H) is applied to a single stone member undergoing the vertical force (P). Here, if the horizontal force exceeds the friction limit state, the deformation continues without increasing the load, as shown in Fig. 10 (b).

The design elements of a single stone member are as follows. P is the vertical force on the block and H is the horizontal force. W is the weight of the block expressed as $\rho(blt)$, where ρ is the unit weight, b is the width of the block, l is the height, and t is the thickness. Therefore, the horizontal force (H_s) at which sliding on a single block commences is $\mu(W+P)$ and the horizontal displacement (δ_s) at that time is $H_s/k_s = \mu(W+P)/k_s$, where k_s is the horizontal stiffness of that surface and μ is the friction coefficient. Tensile force is not a contributing factor when stones are vertically stacked. Thus, when the horizontal force increases, as in Fig. 11, a horizontal force that causes $M_{up} = (P+W)\cdot b/6$ or greater creates an uplift force and the structure becomes unstable. Thus, to model uplift,

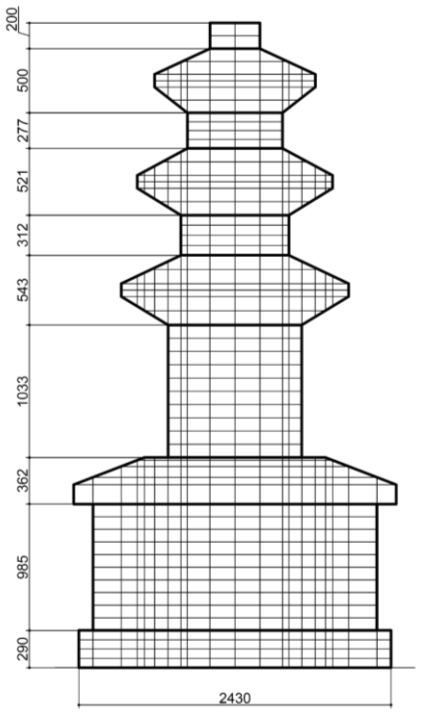

Fig.13 The finite element analytical model

we use a nonlinear element that transmits only compressive (not tensile) force between vertical stones.

A stone pagoda may have several members per floor and stylobates are composed of Jeoksim and Myeonseoks. Thus, this must be considered during structural modeling. However, it is difficult to model and evaluate the seismic behaviors of stone pagodas in three dimensions. Thus, as shown in Fig. 12, we converted the three-dimensional (3D) model into a two-dimensional (2D) finite element model. The overall method was as follows: first, we divided the symmetrical stone pagoda into halves. Second, we applied the layer on a 2D finite element model. Third, we chose finite element thicknesses (T1, T2, and T3) with reference to the perpendicular earthquake data. Fourth, we used the connecting elements (L1, L2, and L3) that transfer only compressive (not tensile) force, considering the areas of surface contact. For example, when T3 was applied, L2 and L3 were also applied to model the contact between the two members. Finally, we applied compressive force only to elements subjected to such force (P1).

The analytical model is shown in Fig. 13. All members were simplified and formalized, and then nodes were created and all elements were subdivided for data accuracy. The upper and lower parts of each member were analyzed in a nonlinear manner, reflecting the nonlinear behaviors of actual surfaces in contact.Since it is a 2D model, one-axis excitation was performed on the X-axis.

3.3.2 Shear stiffness

Shear stiffness, which determines contact surface stiffness, is affected by vertical stress according to the Mohr–Coulomb failure criterion, as shown in Fig. 14.

$$\tau = c + \sigma \tan(\phi) \quad (1)$$

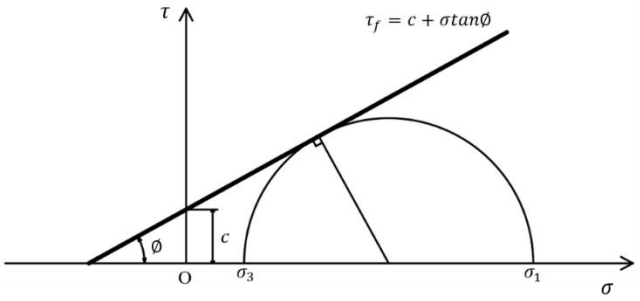

Fig. 14 The Mohr–Coulomb failure criterion

where c is the adhesion, σ is the vertical stress, and $\emptyset$ is the friction angle. In general, shear stiffness is experimentally determined, but it is difficult to reflect the characteristics of contact surfaces in a stone pagoda accurately. Thus, the weight of each member was calculated using the general density of granite, 25 kN/m^3, and the vertical stresses in the lower contact regions were examined. Table 5 shows that the vertical contact stresses were very low, approximately 0.016~0.077 MPa. Therefore, we defined stiffness as the ratio of the average shear stiffness to the contact surface in Eq. (2).

$$K_s = K_{aver} \times A \times A_{ratio} \quad (2)$$

where K_s is the shear stiffness of the contact surface (kN/m), K_{aver} is the average shear stiffness (kN/m^2/m), A is the area of contact surface (m^2), and A_{ratio} is the ratio of areal contact.

The ratio of the average shear stiffness to the contact area varies according to the material, bonding, and weathering conditions. As shown in Table 6, the average shear stiffnesses of contact surfaces ranged from 100,000 to 500,000 kN/ m^2/m and the contact surface ratios ranged from 0.2 to 1.0 when deriving the periods, which thus ranged from 0.066 to 0.202 s. The data of Table 6 were appropriate and applicable because a three-story stone pagoda exhibits a very short periodic structure.

3.3.3 Results

The Gyeongju earthquake caused great deformation in the lower part of the 3F main body stone and the upper part of the 2F roof stone, which, however, remained in contact between the 3F main body stone and 3F roof stone.

Therefore, we applied an average shear stiffness $K_{aver} = 100{,}000\ kN/m^2/m$, a friction coefficient of $\mu = 0.1$, the actual member contact ratio $A_{ratio} = 0.6$ for the general contact surfaces, and a friction coefficient of $\mu = 0.2$ for the contact surface between the top of the 2F roof stone and the bottom of the 3F main body stone. Based on the results of analysis with application of the seismic acceleration shown in Fig. 8, we obtained a single-direction displacement of approximately 60 mm, as shown in Fig. 16, which was smaller than the actual two-way displacement of 90 mm. However, considering that the influences of the vertical component, soil-structure interaction and the distance from the epicenter etc. were large because the epicenter was located only 2.9 km distant, the result is acceptable and applicable.

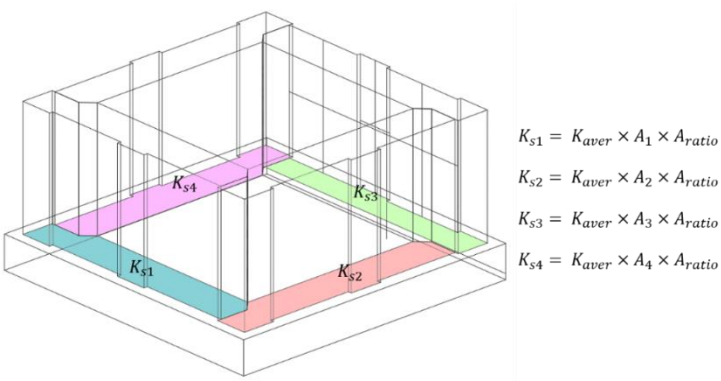

Fig. 15 Shear stiffness of a contact surface

Table 5 Vertical contact stresses of the stone pagoda

Name	Width (m)	Height (m)	Depth (m)	Mass (m^3)	Self-weight (kN)	Cumulative weight (kN)	Contact area (m^2)	Vertical stress (MPa)
3F Roof stone	1.00	0.50	1.00	0.50	12.5	13.8	0.85	0.016
3F Main body	0.92	0.29	0.92	0.25	6.1	19.9	0.85	0.023
2F Roof stone	1.23	0.53	1.23	0.79	19.9	39.7	1.00	0.040
2F Main body	1.00	0.30	1.00	0.30	7.5	47.2	1.00	0.047
1F Roof stone	1.45	0.54	1.45	1.14	28.4	75.6	1.50	0.050
1F Main body	1.23	1.05	1.23	1.57	39.2	114.8	1.50	0.077
Gapseok 2	2.43	0.38	2.43	2.24	56.1	121.9	5.90	0.021
Gapseok 1	1.88	0.99	1.88	3.50	70.0	201.6	3.53	0.057
Myeonseok 4	0.24	0.99	1.09	0.26	6.5	9.0	0.26	0.034
Myeonseok 3	0.24	0.99	0.77	0.18	4.6	6.3	0.18	0.034
Myeonseok 2	1.09	0.99	0.24	0.26	6.5	9.0	0.26	0.034
Myeonseok 1	1.06	0.99	0.24	0.25	6.3	8.7	0.25	0.034
Foundation stone	2.43	0.18	2.43	1.06	13.3	247.9	5.90	0.042

Table 6 First vibration periods of the stone pagoda

Classification		Average shear stiffness of the contact surface, $K_{aver}(kN/m^2/m)$				
		100,000	200,000	300,000	400,000	500,000
Contact area ratio (A_{ratio})	1	0.104 s	0.083 s	0.074 s	0.069 s	0.066 s
	0.8	0.112 s	0.089 s	0.079 s	0.073 s	0.069 s
	0.6	0.126 s	0.097 s	0.085 s	0.079 s	0.074 s
	0.4	0.149 s	0.112 s	0.097 s	0.089 s	0.083 s
	0.2	0.202 s	0.149 s	0.126 s	0.112 s	0.104 s

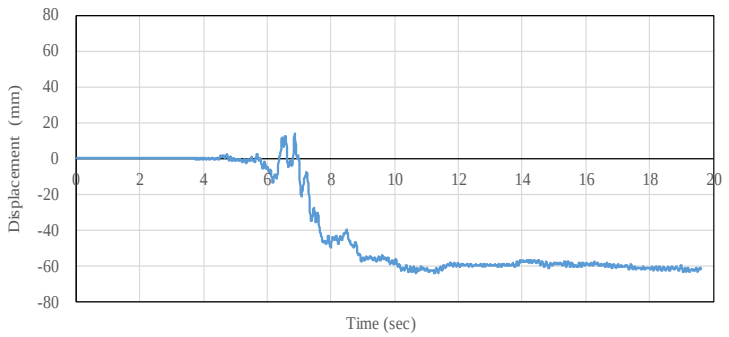

Fig. 16 Displacement of the 3F main body stone

3.4 Discrete element analysis

3.4.1 Analytical model

Stone pagodas are discontinuous structures, because large stones are individually stacked. Thus, finite element analysis may not reveal their precise behaviors. Therefore, we additionally applied discrete element analysis to verify the results of finite element analysis (Melika Naderi and Mehdi Zekavati 2018). We used 3DEC software for the discrete element analysis, which can analyze masonry

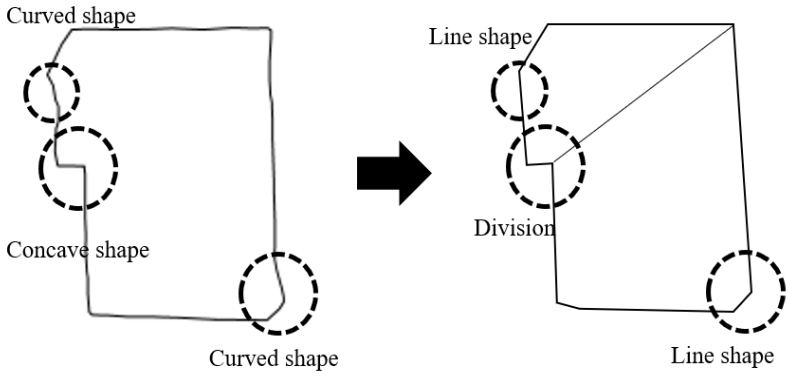

Fig. 17 Member formalization

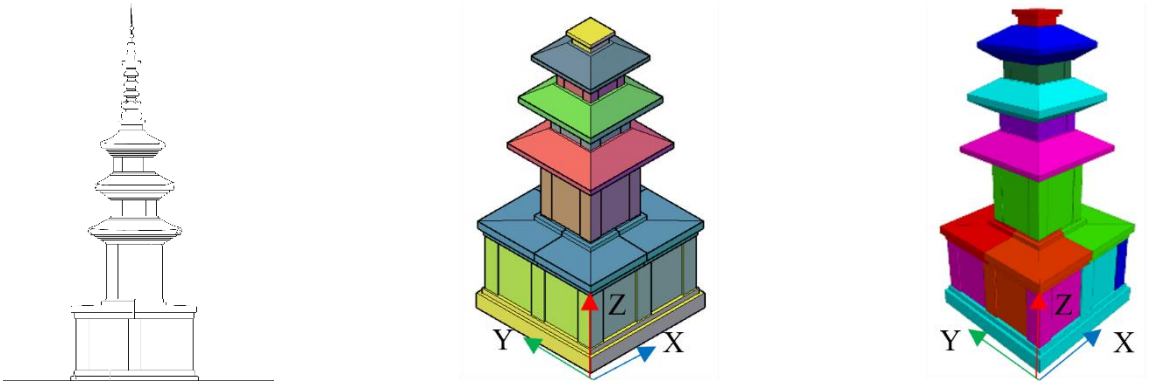

(a) Real-state drawing (b) Structural modeling via CAD (c) Structural modeling via discrete element analysis

Fig. 18 Discrete element modeling process

structures that lack complete adhesion between members and reveal the discontinuous mechanism between contact surfaces (3DEC 2007). The software cannot handle the concavities or curves of raw stone. Thus, for the member formalization shown in Fig. 17, we replaced these shapes using blocks and lines within ranges over which the shapes did not change.

In addition, we modeled the entire stone pagoda with reference to its actual construction. We also performed structural modeling via a computer-aided design (CAD) program using the measured drawings. The structural model for the discrete element analysis is shown in Fig. 18. In addition, uniaxial excitation was performed on the X-axis.

3.4.2 Analytical process and material properties

Discrete element analysis requires multiple steps. First, a CAD drawing is prepared based on actual measurements. The analytical model is run after member formalization via CAD. After modeling, reasonable material properties, boundaries, and load conditions are imposed; structural analysis is performed; and the results are analyzed. In addition, accuracy requires knowledge of the material characteristics of the stones and the contact surfaces. The material properties of Gyeongju granite in Table 7 are based on the values described by Hong *et al.* (2011). The material properties of the contact surfaces were applied based on the shear stiffness $K_{aver} = 100{,}000\ kN/m^2/m$, derived via the finite element analysis.

3.4.3 Results

Discrete element analysis revealed the deformations shown in Fig. 19. Here, the decorative top was most affected. Because the top had no upper load and the contact area with the lower member was small, a large rotational displacement was evident. The 3F main body and roof stones were actually displaced approximately 90 mm westward by the Gyeongju earthquake; the discrete element analysis value was approximately 80 mm, as shown in Fig. 20. This result shows similar behavior to that of the finite element analysis, and is thus also acceptable and applicable.

4. Seismic performance evaluation

We used finite and discrete element analysis to evaluate seismic behaviors during an earthquake. The results of the two analyses did not differ significantly. Finite element analysis is preferable for evaluating seismic performance because it is very time-consuming to use discrete element analysis for nonlinear dynamic behavior. Thus, we used finite element analysis to determine the risks of sliding and rocking in response to seismic events and then identified vulnerable parts of the stone pagoda that were vulnerable to earthquakes.

Table 7 Material properties of stone

Density (kg/m^3)	2,500	Adhesion (MPa)	6.87
Poisson ratio	0.26	Friction angle (°)	52.93
Elastic modulus (GPa)	6.21	Bulk modulus (GPa)	4.30
Compressive strength (MPa)	52.63	Shear modulus (GPa)	2.47
Tensile strength (MPa)	3.70		

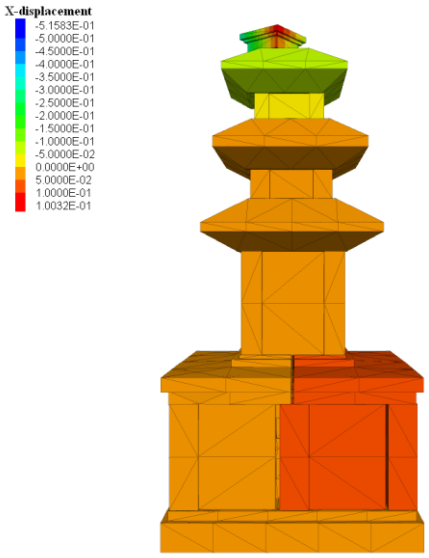

Fig. 19 Deformation revealed by discrete element analysis

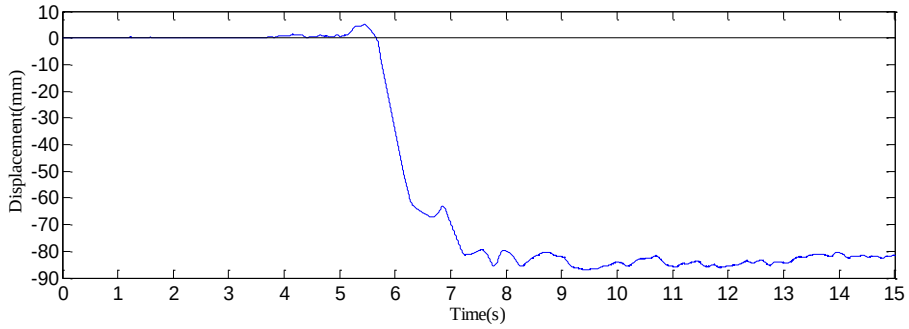

(a) 3F main body stone

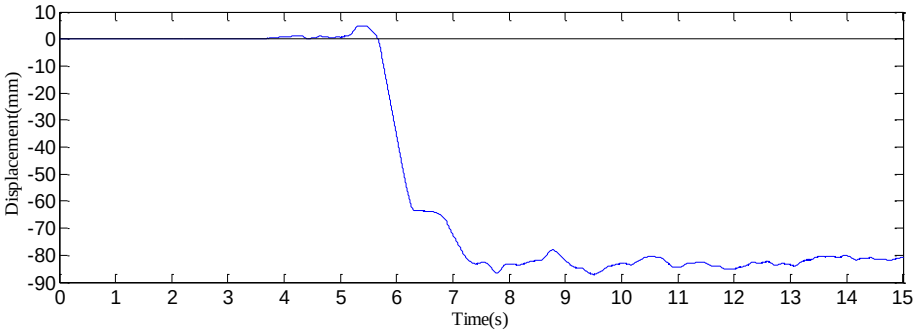

(b) 3F roof stone

Fig. 20 Displacement time history

4.1 Sliding analysis

Sliding analysis can be used to determine whether individual members will slip. We applied the accelerations derived via structural analysis to the masses of the members, and used Newton's law of acceleration to obtain story shear forces as shown in Fig. 21, and identified the forces acting on individual members. Sliding occurs if a

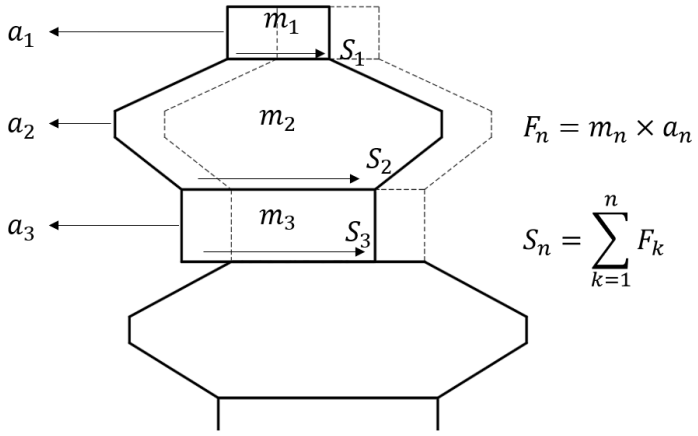

Fig. 21 Modeling sliding

Table 8 Loads on members and critical horizontal forces (CHFs) for sliding

Position	Loading (kN)			Critical horizontal force (kN)		
	Weight (W)	Load (P)	Total	μ = 0.4	μ = 0.5	μ = 0.6
Decorative top	1.05	0	1.05	0.42	0.53	0.63
3F Roof stone	13.31	1.05	14.36	5.74	7.18	8.62
3F Main body	3.58	14.36	17.93	7.17	8.97	10.76
2F Roof stone	21.78	17.93	39.71	15.88	19.86	23.83
2F Main body	5.33	39.71	45.05	18.02	22.53	27.03
1F Roof stone	28.95	45.05	73.99	29.60	37.00	44.39
1F Main body	37.52	73.99	111.51	44.60	55.76	66.91

story shear force exceeds a critical value. However, the coefficients of friction (μ values) between members vary according to the contact surface roughness, and are difficult to estimate. We used friction coefficients ranging from 0.4 to 0.6 based on the surface roughness conditions of granite.

Most sliding was confined to the 3F roof stone and the decorative top; the critical horizontal force was exceeded more often for the roof stone than for the main body stone as shown in Figs. 22(a) and 22(b). Sliding was facilitated because the vertical load at the top was small. The 3F main body stone did not slide extensively, but low-level sliding indicated that the critical horizontal force was briefly exceeded for the 2F and 3F roof stones as shown in Figs. 22(b), 22(c) and 22(d).

4.2 Rocking analysis

Rocking reflects the overturning moment imparted by an earthquake. A member rocking limit is determined by the moment capacity under the member. Elongated and slender structures such as stone pagodas are vulnerable to rocking. When only vertical loads are applied to a member, the forces are compressive (see Fig. 23(a)). (D.K. Kim *et al.*, 2020) When the moments act with the vertical loads, the load distributions are as shown in Fig. 23(b). As the moments increase, the load distributions change to the distributions shown in Fig. 23(c). When compressive stress is zero on the left but maximum on the right, a critical state without uplift develops. The moment at this critical state corresponds to the resistive moment. If the load distribution is triangular, the load is applied at 1/3 of the member width (L_f); the distance from this point to the centroid is 1/6 of the member width. Thus, the moment resistance (i.e., the overturning moment) of each member is given by Eq. (3).

$$M_{uplift} = \frac{\sum_{n=1}^{i} W_n \times L_f}{6} \quad (3)$$

where W is the total weight between the upper and lower members, L_f is the width of the contact surface of the bottom member, i is the top member number, and n is the number of the member under evaluation.

With the exception of the decorative top, all members exceeded the moment resistance limit. The moment resistance of the decorative top was low because the weight and length of the contact surface were smaller than those of other members. In particular, the limit line of moment resistance was greatly exceeded near the bottom, because the lower members were more elongated and slender than the upper members. During actual earthquakes, lower members are generally more vulnerable to overturning, but do not exhibit large deformations because the vertical loads are large. The 3F main body and roof stones were the members that experienced the most damage because the limits of both rocking and sliding were exceeded.

4.3 Risk analysis

Although risk analysis of horizontal displacement due to earthquake loads is essential, no standard for allowable criteria is available because stone pagodas assume various forms and are built in various manners. Thus, we used the

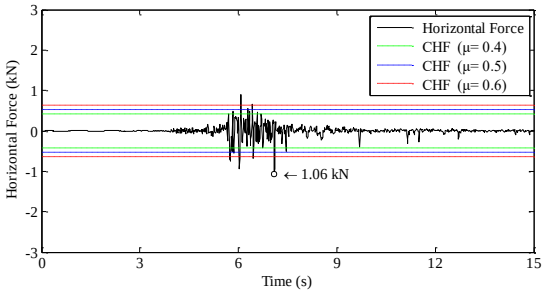

(a) Decorative top

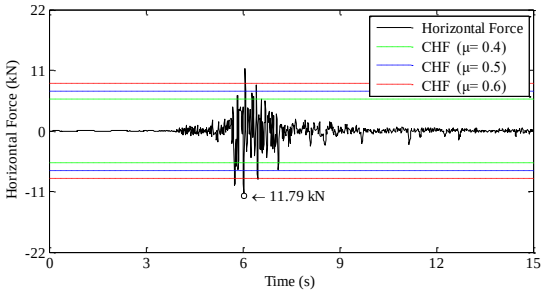

(b) 3F roof stone

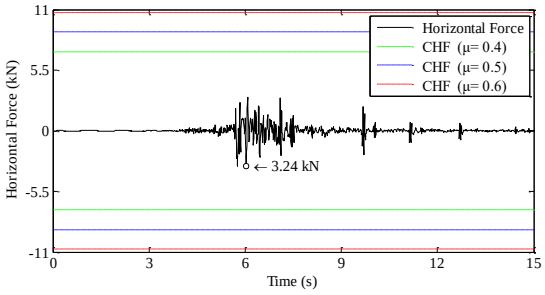

(c) 3F main body stone

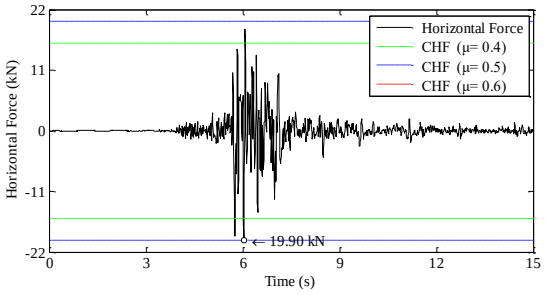

(d) 2F roof stone

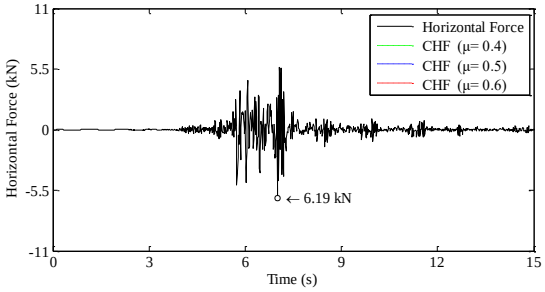

(e) 2F main body stone

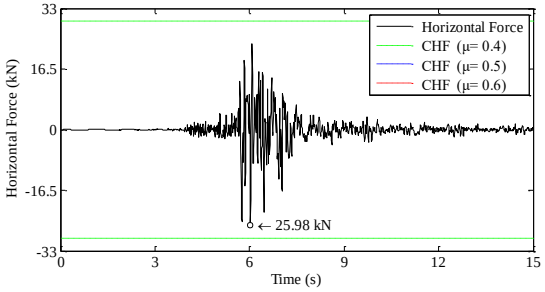

(f) 1F roof stone

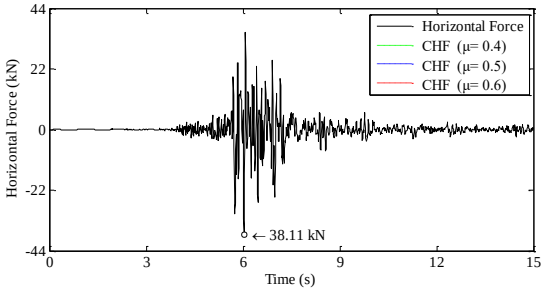

(g) 1F main body stone

Fig. 22 Time histories of story shear forces for all members

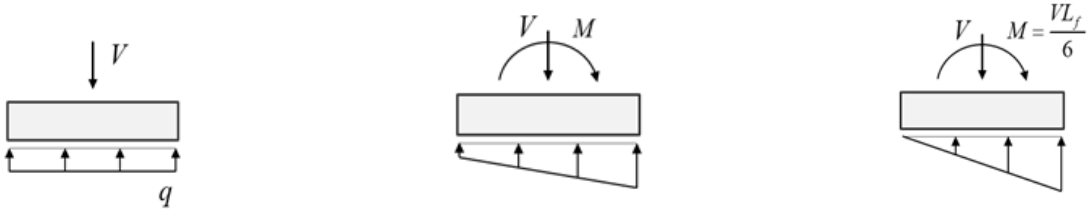

(a) Initial state (b) Elastic state prior to uplift (c) Elastic state at uplift

Fig. 23 Limitations on member uplift

story deformation criteria for unreinforced masonry structures. After the horizontal displacements of all members have been obtained by analysis, the story deformation angles are calculated as shown in Fig. 26.

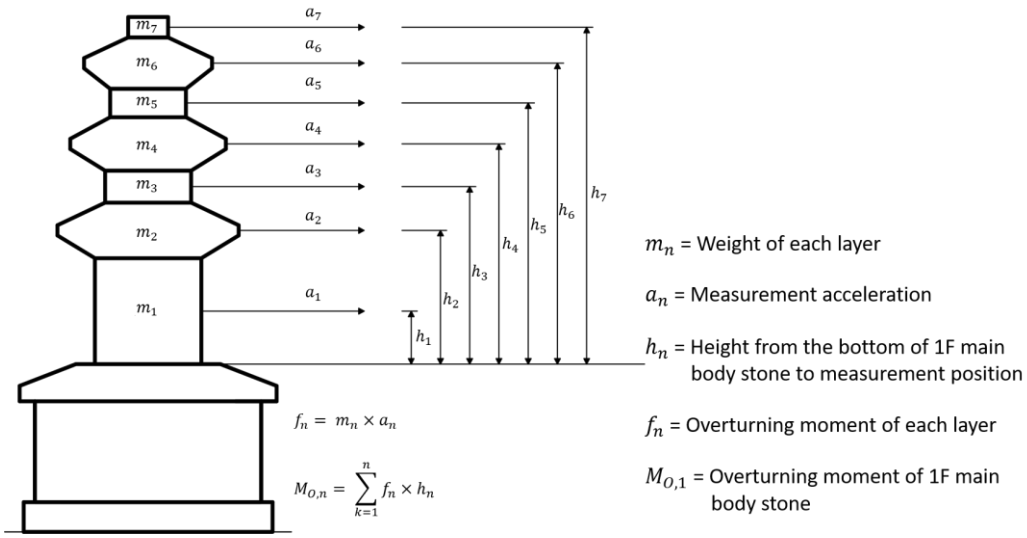

Fig. 24 Calculation of the overturning moments

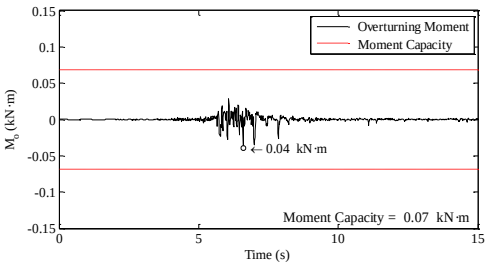

(a) Decorative top

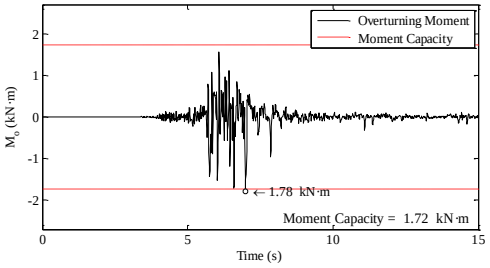

(b) 3F roof stone

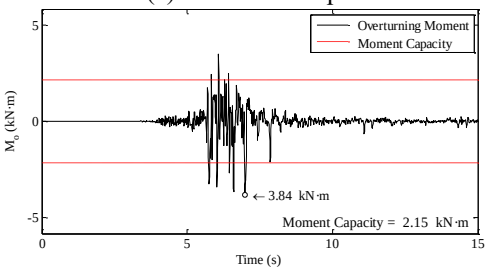

(c) 3F main body stone

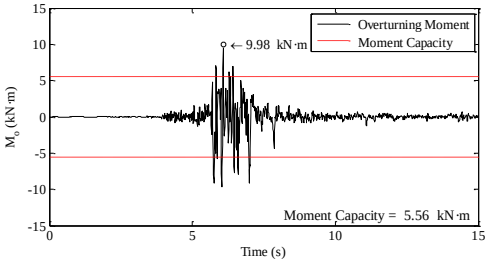

(d) 2F roof stone

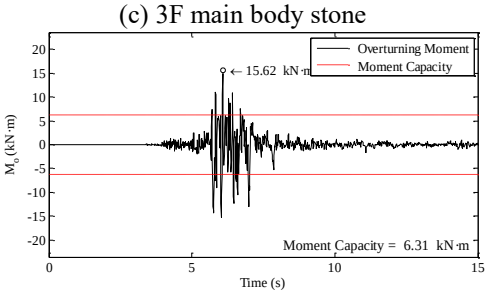

(e) 2F main body stone

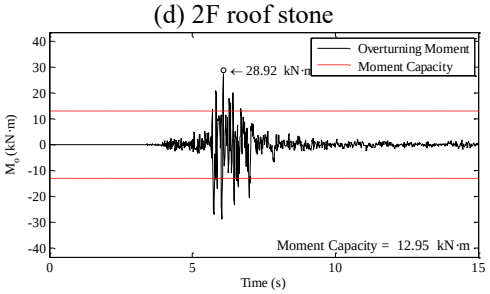

(f) 1F roof stone

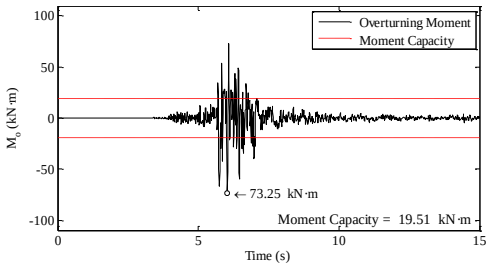

(g) 1F main body stone

Fig. 25 Time histories of overturning moments for all members

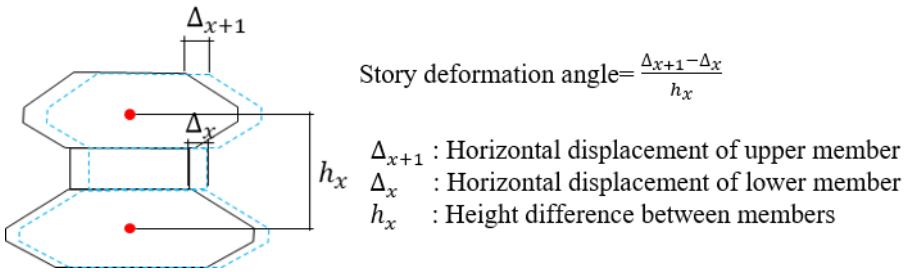

Fig. 26 Story deformation angles by relative displacements

Table 9 Allowable story deformation angles according to performance levels (FEMA 356 2000)

Structural system	Earthquake-resistant design		
	Immediate occupancy	Life safety	Collapse prevention
RC moment frame	0.7	2	3
RC moment frame with masonry wall	0.5	1	1.5
RC shear wall with shear wall system	0.25	0.5	1
RC shear wall with bending-dominant system	0.5	1	2
Unreinforced masonry shear wall system	0.3	0.6	1
Steel frame	0.7	2.5	4
Steel frame with bracing	0.5	1.5	2

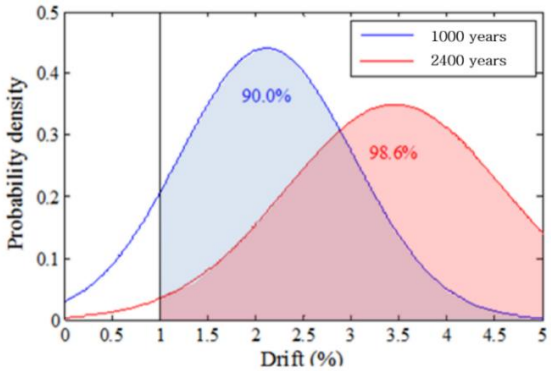

Fig. 27 Probability of collapse from structural damage

Table 10 Earthquake records

EQ no.	Name	Country	Year	Station	Magnitude	Distance (km)	Scale factor
1	Montenegro	Serbia and Montenegro	1979	Ulcinj-Hotel	6.9	21	1.71
2	Kocaeli	Turkey	1999	Gebze	7.5	11	1.45
3	Izmit	Turkey	1999	Gebze-Tubit	7.6	47	1.70
4	Montenegro	Serbia and Montenegro	1979	Hercegnovi	6.9	65	1.74
5	Parkfield-02	USA	2004	Parkfield	6.0	5	0.42
6	San Fernando	USA	1971	Pasadena	6.6	22	3.30
7	Kremidia (aftershock)	Greece	1984	Pelekanada	5.0	16	0.55
8	Kozani	Greece	1995	Kozani-Prefecture	6.5	17	2.29
9	Izmit	Turkey	1999	Izmit-Meteoroloji	7.6	9	0.81
10	Northridge-01	USA	1994	Vasquez	6.7	24	1.26
11	Kocaeli	Turkey	1999	Izmit	7.5	7	1.50
12	Campano Lucano	Italy	1980	Sturno	6.9	32	0.69
13	Tottori	Japan	2000	SMNH10	6.6	16	2.56
14	Friuli (aftershock)	Italy	1977	Somplago	5.4	9	1.56
15	Northridge-01	USA	1994	LA - Wonderland Ave	6.7	20	0.99
16	Bingol	Turkey	2003	Bingol-Bayindirlik	6.3	14	2.06
17	Kalamata	Greece	1997	Koroni-Town Hall	6.4	48	2.28
18	Friuli (aftershock)	Italy	1976	Tarcento	5.3	8	2.34
19	San Fernando	USA	1971	Lake Hughes	6.6	24	2.05
20	Friuli	Italy	1976	Tolmezzo-Diga	6.5	23	2.94

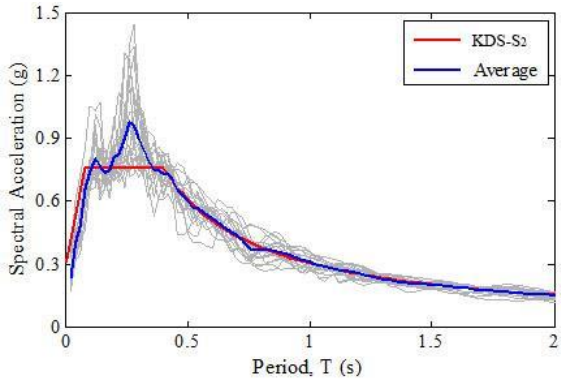

Fig. 28 Average response spectra of 20 earthquakes adjusted to 0.22 g

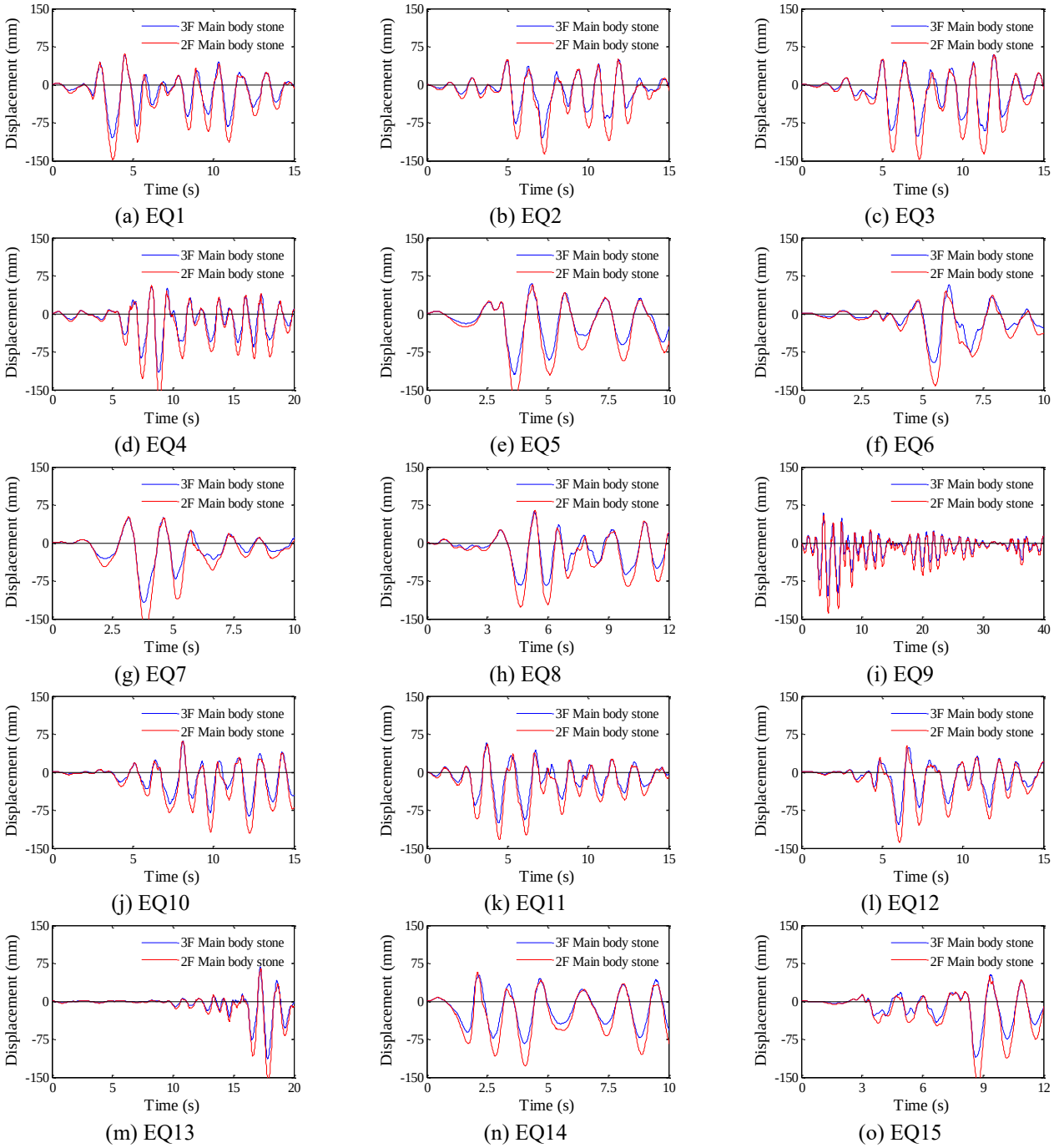

(a) EQ1 (b) EQ2 (c) EQ3

(d) EQ4 (e) EQ5 (f) EQ6

(g) EQ7 (h) EQ8 (i) EQ9

(j) EQ10 (k) EQ11 (l) EQ12

(m) EQ13 (n) EQ14 (o) EQ15

Fig. 29 Continued

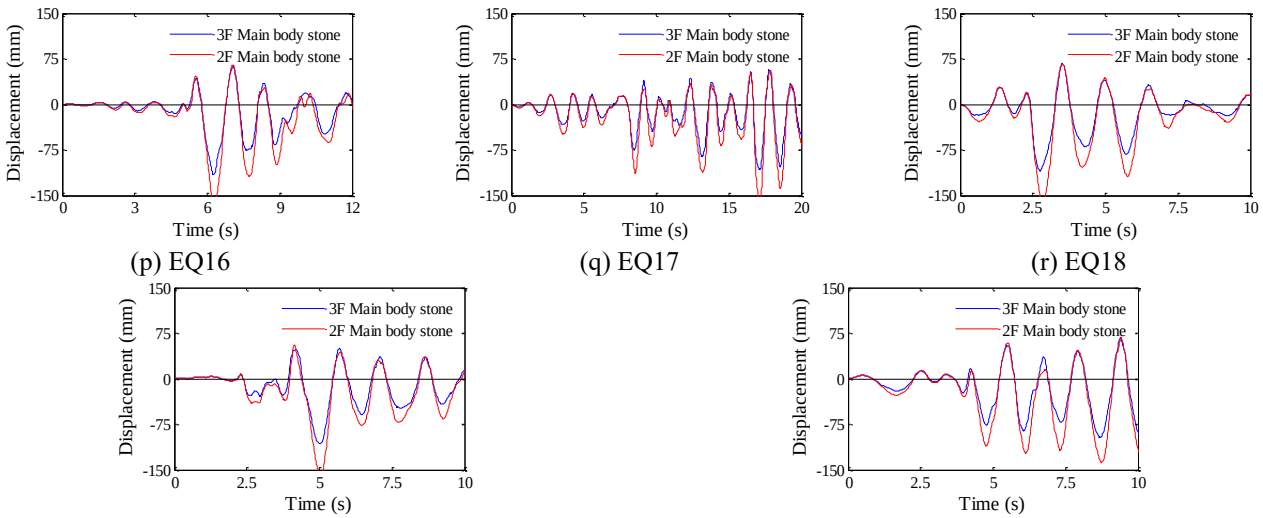

(p) EQ16 (q) EQ17 (r) EQ18

(s) EQ19 (t) EQ20

Fig. 29. Displacement time histories for the 3F and 2F main body stones

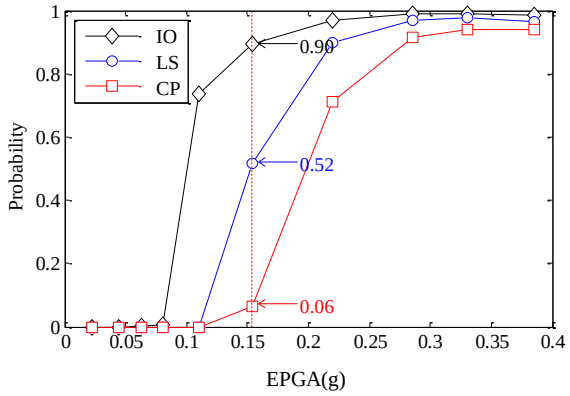

Fig. 30 Fragility curve of the three-story stone pagoda at Cheollyongsa temple site

The FEMA 356(2000), ATC-40(1996), and KDS 41 17 00(2019) criteria are used to evaluate the seismic performance of existing buildings. However, because there is no standard by which to determine the seismic performance of a stone pagoda, we used the criteria applicable to a general building unreinforced masonry shear wall system. At the immediate occupancy (IO) level, structures experience minor cracks in non-structural elements. At the life safety (LS) level, structures have residual stiffness and strength in all stories, but with permanent drift. Finally, at the collapse prevention (CP) level, structures have minimal stiffness and strength in all stories, but columns and walls remain standing. Thus, we assumed that a stone pagoda will be destroyed if the allowable story deformation angle at the CP level is exceeded.

A probability density of 1.0 predicts the collapse of a stone pagoda structure, based on the allowable story deformation angle at the CP level for an unreinforced masonry shear wall system. By dividing the area over which the probability density function exceeds 1 by the total area, the collapse probability of Fig. 27 can be derived with reference to the return period. The probability density function is given by Eq. (4).

$$P(x) = \frac{1}{\sqrt{2\pi\sigma^2}} \times \sqrt{\frac{(x-m)^2}{2\sigma_x^2}} \tag{4}$$

where σ is the average story deformation angle and m is the standard deviation thereof.

Input seismic waves were collected from PEER (2021), USGS (2021), and ESMD (2021) as shown in Table 10 and then adjusted with reference to the rock spectrum of the Korea design standard (KDS 41 17 00, 2019).

Unlike Japan, Mexico, and the west coast of the United States, the depth of most Korean soils is less than 20 m (to bedrock). We thus used this depth, and subdivided by 5 m to reflect gradual increases with depth in soil quantity, deposits, weathered soil, and weathered rock. Fig. 28 shows the average response spectrum of the seismic records amplified by the representative ground conditions of KDS 41 17 00: 2019; thus S_2 ground of depth less than 20 m. The seismic waves were amplified in the period of 0.2~0.3 s. The displacement time histories of the 3F and 2F main body stones for the 20 seismic waves are shown in Fig. 29.

The fragility curve of Fig. 30 was derived by subjecting each of the 20 seismic waves to nonlinear dynamic analysis at each of 10 seismic levels. We then calculated the story deformation angles (as shown in Fig. 26) using the displacement values of the 2F and 3F main body stones. Finally, we calculated the pagoda collapse probability using the area over the allowable story deformation angle during the seismic performance step of the probability density graph (Fig. 27).

The collapse probability was very small up to 0.1 g, but increased dramatically thereafter, as shown in Fig. 30. During an earthquake of more than 0.3 g, the probability of collapse exceeded 80%. Because the return period of the Gyeongju earthquake is approximately 1,000 years (earthquake peak ground acceleration [EPGA] = 0.154 g), the risks of collapse of the three-story stone pagoda at an

EPGA of 0.154 g are 90%, 52%, and 6% at the IO, LS, and CP levels. The pagoda did not collapse during the Gyeongju earthquake, but the 3F main body and roof stones rotated and slid, reflecting seismic performance at the LS level. In a stone pagoda, stones are stacked individually, and the contact area decreases toward the top. Thus, a more severe earthquake is associated with a greater probability of collapse from the top.

5. Conclusions

The damages to stone pagodas by the Gyeongju earthquake were analyzed and structural models reflecting the actual responses of a three-story stone pagoda at the Cheollyongsa temple site were derived. Then, stone sliding and rocking, and the collapse risk were analyzed. The conclusions are as follows.

• Finite element modeling and analysis were performed at various shear stiffness and friction values for the behavior of a three-story stone pagoda at the Cheollyongsa temple site. When we applied an average shear stiffness of K_{aver} of 100,000 $kN/m^2/m$, a friction coefficient μ of 0.1, and an actual member contact ratio (A_{ratio}) of 0.6, displacement of approximately 60 mm occurred in a single direction; the actual displacement due to earthquake was 90 mm. However, considering the vertical component of the earthquake and the short distance from the epicenter, the finite element analysis results are acceptable and applicable.

• Because stone pagodas are structures with discontinuous contact surfaces, it is difficult to precisely model their behavior via finite element analysis alone. Thus, we also employed a discrete element analysis model to reflect the discontinuous characteristics. The input conditions were the same as used in the finite element analysis model, the applicability of which was checked by comparing the results. The modeled single-direction displacement of the 3F main body stone was 80 mm, similar to the actual displacement of 90 mm. Thus, the results of the two analyses did not differ significantly. Therefore, we applied finite element analysis to evaluate the seismic performance because discrete element analysis for nonlinear dynamic behavior is very time-consuming.

• The Gyeongju earthquake has a return period of approximately 1,000 years (EPGA = 0.154 g). We retrieved earthquake records and found that acceleration responses of extreme short-period structures of less then 0.2s were larger than the spectrum acceleration of the Korean seismic design standard. Thus, short-period structures (e.g., stone pagoda structures) were severely damaged by the Gyeongju earthquake, which exhibited extreme short-period characteristics.

• Stone sliding developed principally in the upper region, because the vertical load decreased upward. Most rocking developed in the lower region, because the lower members were more slender than others. The 3F main body and roof stones were particularly vulnerable because both the rocking and sliding limits were exceeded.

• Various seismic waves and levels for structural analysis were applied and risk analysis by means of a fragility curve was performed. Because a stone pagoda is a masonry structure, it is vulnerable to lateral forces, and the collapse risk increases substantially as earthquake intensity increases. Because the return period of the Gyeongju earthquake is approximately 1,000 years, the risks of collapse of the stone pagoda structure for an EPGA of 0.154 g are 90%, 52%, and 6% at the IO, LS, and CP levels. The pagoda did not collapse during the Gyeongju earthquake, but the 3F main body and roof stones rotated and slid. Thus, it was found out that the seismic performance of the pagoda is consistent with the LS level.

Acknowledgments

This research was supported by the National Research Foundation of Korea (NRF) grant funded by the Korea government (MSIT) (No. 2019R1F1A1057903). The authors would like to express sincere gratitude for their support.

References

Preciado, A., Bartoli, G. and Ramírez-Gaytán, A. (2017), "Earthquake protection of the Torre Grossa medieval tower of San Gimignano, Italy by vertical external prestressing", Eng. Fail. Anal., **71**, 31-42. https://doi.org/10.1061/(ASCE)CF.1943-5509.0000746.

ATC-40 (1996), *Chapter 4: Seismic Hazard, Seismic Evaluation and Retrofit of Concrete Buildings*, Seismic Safety Commission, State of California, U.S.A.

Kim, D.K., Park, H.G., Kim, D.S. and Lee, H. (2020), "Nonlinear system identification on shallow foundation using Extended Kalman Filter", *Soil Dyn. Earthq. Eng.*, **128**, 105857. https://doi.org/10.1016/j.soildyn.2019.105857.

European Strong-Motion Database (ESMD) (2021), *The European Strong-Motion Database*, https://www.isesd.hi.is/

FEMA 356 (2000), *Chapter 2: General Requirements, Prestandard and commentary for the seismic rehabilitation of buildings, Federal Emergency Management Agency*, Washington, DC, U.S.A.

Peña, F., Lourenço, P.B., Mendes, N. and Oliveira, D.V. (2010), "Numerical models for the seismic assessment of an old masonry tower", *Eng. Struct.*, **32**(5), 1466-1478. https://doi.org/10.1016/j.engstruct.2010.01.027.

Micelli, F. and Cascardi, A. (2020), "Structural assessment and seismic analysis of a 14th century masonry tower", *Eng. Fail. Anal.*, **107**, 104198. https://doi.org/10.1016/j.engfailanal.2019.104198.

KDS 41 17 00 (2019), *Seismic Building Design Code. Ministry of Land, Infrastructure and Transport (MOLIT)*, Sejong, Korea

Jeong, K.H. and Lee, H.S. (2018), "Ground-motion prediction equation for South Korea based on recent earthquake records", *Earthq. Struct.*, **15**(1), 29-44. http://dx.doi.org/10.12989/eas.2018.15.1.029.

Adam, M.A., El-Salakawy, T.S., Salama, M.A. and Mohamed, A.A. (2020), "Assessment of structural condition of a historic masonry minaret in Egypt", *Case Studies Construct. Mater.*, **13**,

e00409. https://doi.org/10.1016/j.cscm.2020.e00409.
Hejazi, M., Moayedian, S.M. and Daei, M. (2016), "Structural analysis of Persian historical brick masonry minarets", *J. Perform. Construct. Facili.*, **30**(2), 04015009. https://doi.org/10.1061/(ASCE)CF.1943-5509.0000746.
Naderi, M. and Zekavati, M. (2018), "Assessment of seismic behavior stone bridge using a finite element method and discrete element method", *Earthq. Struct.*, **14**(4), 297-303. http://dx.doi.org/10.12989/eas.2018.14.4.297.
Ministry of Public Safety and Security (2017), *9.12 Earthquake Whitepaper*, Ministry of Public Safety and Security, Sejong, Korea
Yurdakul, M., Yılmaz, F., Artar, M., Can, Ö., Öner, E. and Daloğlu, A.T. (2021), "Investigation of time-history response of a historical masonry minaret under seismic loads", *Struct.*, **30**, 265-276). https://doi.org/10.1016/j.istruc.2021.01.008.
National Research Institute of Cultural Heritage (NRICH) (2009), *Stone pagoda of Gyeongsangbuk-do III (in Korean), National Research Institute of Cultural Heritage (NRICH)*, Deajeon, Korea.
OpenSees (2020), *Open System for Earthquake Engineering Simulation*, https://opensees.berkeley.edu/
Pacific Earthquake Engineering Research Centre (PEER) (2021), Strong motion database, http://ngawest2.berkeley.edu/
Hong, S.I., Shin, H.B., Kim, D.M. and Kim, H.S. (2011), "Structural behavior evaluation according to roughness of discontinuum surface of stone pagoda", *Architect. Institutue Korea*, **27**(10), 63-70. https://doi.org/10.5659/JAIK_SC.2018.34.6.19.
Altiok, T.Y. and Demir, A. (2021), "Collapse mechanism estimation of a historical masonry minaret considered soil-structure interaction", *Earthq. Struct.*, **21**(2), 161-172. http://dx.doi.org/10.12989/eas.2021.21.2.161
Three-dimensional distinct element code(3DEC) (2007), *Itasca Consulting Group, Mimmeapolis*, U.S.A. https://www.itascacg.com/software/3DEC
United States Geological Survey (USGS) (2021), Earthquake Hazards Program, https://earthquake.usgs.gov/

DK